論文 / 著書情報
Article / Book Information

Title	Analyzing Deformation of a Cationic Photopolymerized Epoxy Adhesive during the Curing Process in UV Irradiation and Dark Reaction based on Finite Element Method and Measurement
Authors	Akari Takahashi, Yu Sekiguchi, Nobuhiro Taki, Masahiro Okamura, Chiaki Sato
Citation	The Journal of Adhesion, Vol. 100, pp. 599-615
Pub. date	2023, 7
Creative Commons	Information is in the article.

THE JOURNAL OF ADHESION
2024, VOL. 100, NO. 7, 599–615
https://doi.org/10.1080/00218464.2023.2238611

Taylor & Francis
Taylor & Francis Group

Analyzing Deformation of a Cationic Photopolymerized Epoxy Adhesive during the Curing Process in UV Irradiation and Dark Reaction based on Finite Element Method and Measurement

A. Takahashi[a,b], Y. Sekiguchi[c], N. Taki[d], M. Okamura[d], and C. Sato[c]

[a]Laser and Photonics Research Department, Optical Technologies R&D Center, Fujikura Ltd, Chiba, Japan; [b]Department of Mechanical Engineering, School of Engineering, Tokyo Institute of Technology, Yokohama, Japan; [c]Institute of Innovative Research, Tokyo Institute of Technology, Yokohama, Japan; [d]JSOL Corporation, Analysis Technology Department, Tokyo, Japan

ABSTRACT

In the manufacturing of optical products, precise adjustments are made to maintain the optical axis alignment of optical components, which are then securely positioned using adhesives. To achieve positional accuracy at the micron level, it is essential to comprehend the deformation of the adhesive joint over time during processing. This study focuses on investigating the displacement of optical components resulting from the deformation of a cationic photopolymerized epoxy adhesive, which cures under ultraviolet (UV) radiation. First, the conversion of the adhesive was formulated based on a curing reaction model. This conversion can be divided into three stages: the initial reaction during UV irradiation, the subsequent dark reaction, and the reaction induced by heating. Moreover, formulations were developed to describe changes in curing shrinkage, thermal expansion, and viscoelasticity in relation to the conversion. These equations, governing the adhesive properties, were then used to perform finite element method (FEM) simulations to analyze the position of the optical component. Experimental tests on adhesively bonded components were conducted under conditions identical to those employed in the simulation. Throughout the curing process of the adhesive, the optical component was continuously imaged using a coherence-scanning interferometer, enabling the quantification of its displacement from the acquired images. The results of the FEM simulation and experimental analysis exhibited a consistent trend, indicating the effectiveness of the modeling and simulation methods employed in this study. The majority of the displacement of the optical component occurred over several hours during the dark reaction stage, rather than during UV irradiation. Notably, the movement of the optical component was not limited solely to the thickness direction of the adhesive layer because of curing shrinkage but also extends to the in-plane direction because of the non-uniform distribution of the UV irradiation intensity.

ARTICLE HISTORY
Received 4 June 2023
Accepted 16 July 2023

KEYWORDS
UV-curable adhesive; conversion; curing degree; curing shrinkage; viscoelasticity; finite element method (FEM); finite element analysis (FEA)

CONTACT A. Takahashi akari.takahashi@jp.fujikura.com Laser and Photonics Research Department, Optical Technologies R&D Center, Fujikura Ltd, 1440 Mutsuzaki, Sakura-shi, Chiba 285-8550, Japan

1. Introduction

In the manufacturing process of optical products, several optical components such as lenses and mirrors are fixed to their housing to construct spatial optics. Precise alignment along the optical axis must be maintained for these components. UV-curable adhesives are commonly used to fix these components. As the name suggests, these adhesives can be cured under UV irradiation within a short period. However, the expansion and shrinkage of the adhesive layers can cause displacement of the components from their original positions, leading to degradation of their optical characteristics. Achieving micron-scale positional accuracy for these components is crucial, making high-precision adhesion indispensable for the development of optical products.[1–4]

Understanding the curing process of adhesives is essential to achieving precise adhesion. The curing process involves more than simple shrinkage due to the curing reaction; it also entails significant changes in mechanical properties, such as a transition from a viscous to a viscoelastic state. This process can have long-term effects on positional variation because of the relaxation of internal stresses caused by curing.

Previously, numerous product prototypes had to be developed to optimize adhesive configuration, dimensions, and processing conditions. To realize optical products with high performance and reliability in a shorter timeframe, there is a need for a method to quantitatively predict the deformation and internal stress of adhesive parts under arbitrary curing conditions. This can be achieved by modeling the physical properties of adhesives subjected to curing.

Several studies have reported models for the curing reaction of adhesives[5–16] and the changes in the physical properties during the curing process.[17–22] Most of these studies have focused on heat-curable resins and radical polymerization UV-curable resins. Cationic polymerization UV-curable adhesives are also often used for optical products because of their advantages over radical polymerization adhesives, such as a smaller curing shrinkage, no oxygen inhibition, and superior heat resistance. However, few studies have modeled the curing reaction for cationic polymerization UV-curable adhesives,[14–16] and few researchers have formulated the deformation associated with curing for these adhesives.

In the previous paper, we reported on modeling the changes in physical properties of the cationic polymerization UV-curable adhesive during curing.[23] This study entailed a finite element analysis (FEA) investigation on the displacement of a glass component on a metallic substrate bonded to an adhesive in an optical system. Our analysis is based on a model of the physical properties of the adhesive. Experiments were performed under the same conditions as the simulation, in which the displacements of the glass component were continuously measured in situ using an optical method. The

material modeling and analytical methods were validated by comparing the results of simulations and experiments.

2. Simulations and experiments

2.1. Modeling of adhesive joints

This study employed an epoxy resin-based cationic polymerization-type adhesive for precise adhesion. This type of adhesive is appropriate for the fabrication of optical products due to the small shrinkage during curing and the low coefficient of thermal expansion.[24,25] The adhesive was filled with a silica filler to minimize expansion and shrinkage. The adhesive contained an iodonium salt-type photocationic polymerization initiator and a curing agent that reacted with heat and was cured through UV irradiation and heating.[26]

The conversion of the adhesive was measured using the fluorescence method (OL201MS, AcroEdge, Japan), and the parameters were derived by fitting the data. In our previous paper,[23] the parameters of the adhesive were measured under different curing conditions from this paper, so the parameters have been determined again although they are less sensitive to curing conditions. There are two reaction mechanisms for this adhesive: UV irradiation and heating. Previous studies have suggested that photocationic reactions involve two stages.[15,16] Therefore, this reaction must be formulated in a total of three stages. There was an initial curing reaction associated with UV irradiation (p_{uv}), a dark reaction after UV irradiation (p_{h1}), and a reaction due to the curing agent that reacted with heat (p_{h2}) in the conversion of the adhesive. The n$^{\mathrm{th}}$ order model, which was proposed by Martin et al.,[5,6] was applied to each stage, and their superposition was used as the overall reaction system by following the method proposed by Chiou et al.[7] They can be expressed as

$$\frac{dp_{\mathrm{uv}}}{dt} = K_{\mathrm{uv}}(1-p) \tag{1}$$

$$K_{\mathrm{uv}} = k_{\mathrm{uv}} \exp\left(\frac{-c_{\mathrm{uv}}}{RT}\right) = k_{\mathrm{uvT}} I^{M} \exp\left(\frac{-c_{\mathrm{uv}}}{RT}\right) \tag{2}$$

$$\frac{dp_{\mathrm{h1}}}{dt} = K_{\mathrm{h1}}(1-p) \tag{3}$$

$$K_{\mathrm{h1}} = k_{\mathrm{h1}} \exp\left(\frac{-c_{\mathrm{uv}}}{RT}\right) = k_{\mathrm{h1T}} I_{\mathrm{t}}^{N} \exp\left(\frac{-c_{\mathrm{uv}}}{RT}\right) \tag{4}$$

$$\frac{dp_{\mathrm{h2}}}{dt} = K_{\mathrm{h2}}(1-p) \tag{5}$$

$$K_{h2} = k_{h2}\exp\left(\frac{-c_h}{RT}\right) \tag{6}$$

Here, I is the UV light intensity, I_t is the UV-integrated light intensity, t is the time, and T is the temperature. k_{uvT}, M, c_{uv}, k_{h1T}, N, k_{h2}, and c_h are experimentally determined constants. The relationship between the rate constants (k_{uv}, k_{h1}) and UV-integrated light intensity is expressed by a power expression,[14] as shown in Equation 2 and Equation 4. The model has experimentally been validated because this study concerned the conversion during the dark reaction process which was not discussed in detail in our previous paper. Conversions p_{uv} and p_{h1} are shown in Figures 1 (a) and (b), respectively.

The validation procedure of models for conversion and properties of the adhesive was described in our previous paper.[23] The changes in the

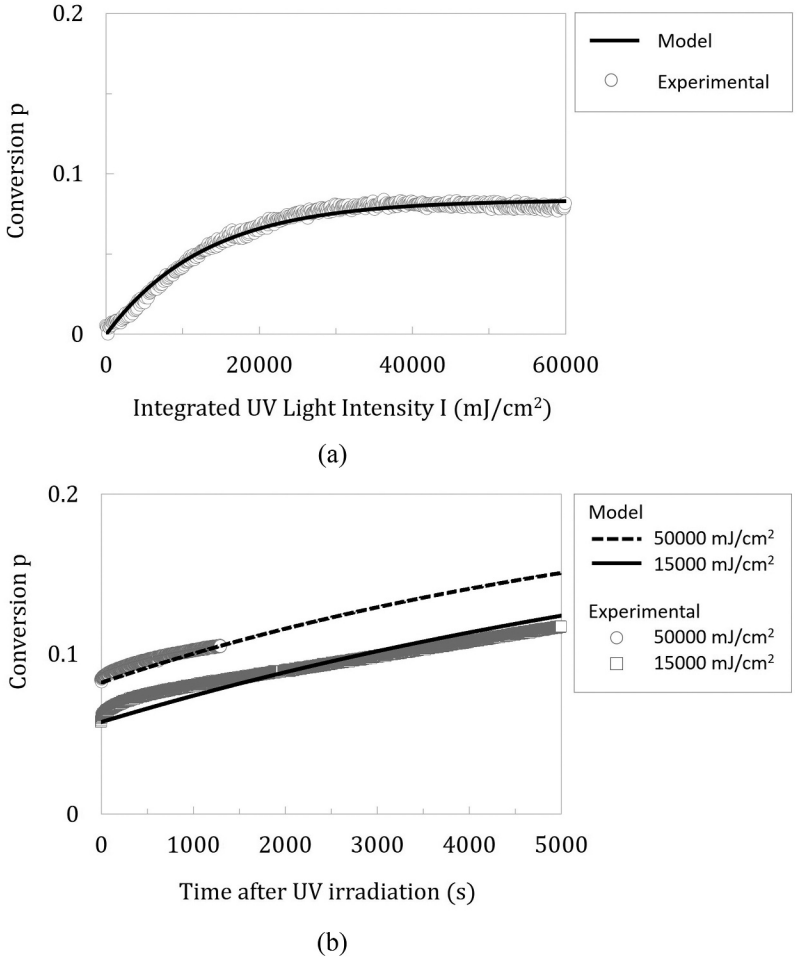

Figure 1. Conversion of the adhesive. (a) Conversion during UV irradiation, (b) Conversion after UV irradiation.

viscoelasticity, curing shrinkage, and thermal expansion were measured and formulated by fitting them to the data associated with the conversion. The shear moduli were measured using a rotational rheometer with a UV-curing function (MCR302, Anton Paar, Austria). The curing shrinkage and coefficient of linear expansion were measured using a laser displacement meter (EU201, AcroEdge, Japan). The changes in the storage and loss moduli can also be expressed by equations (7) - (9) in three stages that mostly correspond to the three stages of curing (p_{uv}, p_{h1}, and p_{h2}). The relationship between the conversion and moduli is shown in Figure 2.

$$G = A_1 \exp(B_1 p)(p < 0.04) \tag{7}$$

$$G = A_2 \exp(B_2 p)(0.04 < p < 0.15) \tag{8}$$

$$G = A_3 (1 - \exp(-B_3 p))(p > 0.15) \tag{9}$$

In Equations (7) - (9), A_1, B_1, A_2, B_2, A_3, and B_3 are constants that must be determined experimentally. When the conversion is 0.04 or less, it is defined as stage 1 in which gelation is yet to occur. The elastic modulus increases rapidly during this stage. When the conversion is within 0.04–0.15, it is defined as stage 2; the increase in the elastic modulus decelerates. Stage 3 occurred when the conversion exceeded 0.15; the elastic modulus was almost saturated.

For the curing shrinkage and coefficient of linear expansion, the three stages of the reaction were fitted to a sigmoid curve, as shown in Equation 17 and Equation 17. The relationship between the conversion and curing shrinkage is plotted in Figure 3, and the relationship between the conversion and coefficient of linear expansion is shown in Figure 4.

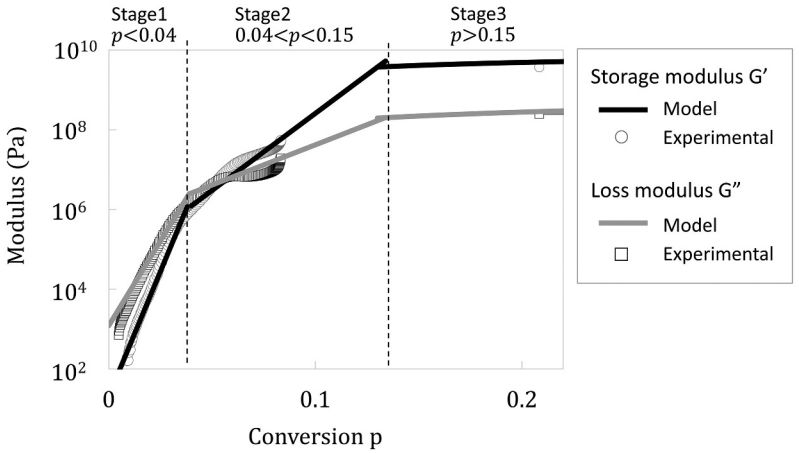

Figure 2. Relationship between the moduli and the conversion.

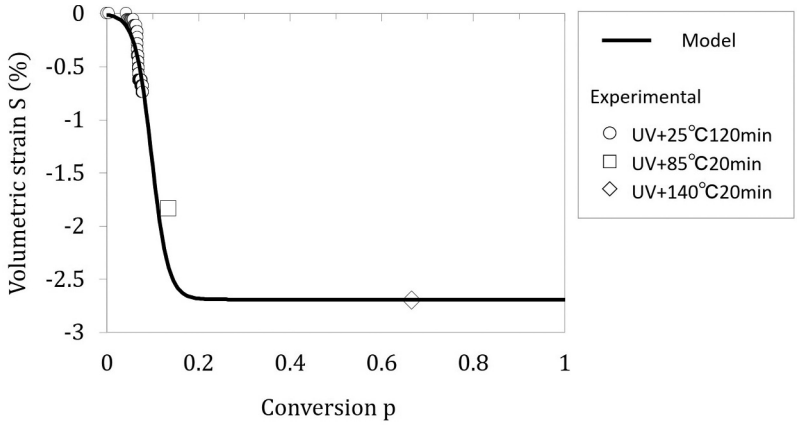

Figure 3. Relationship between the volumetric strain and the conversion.

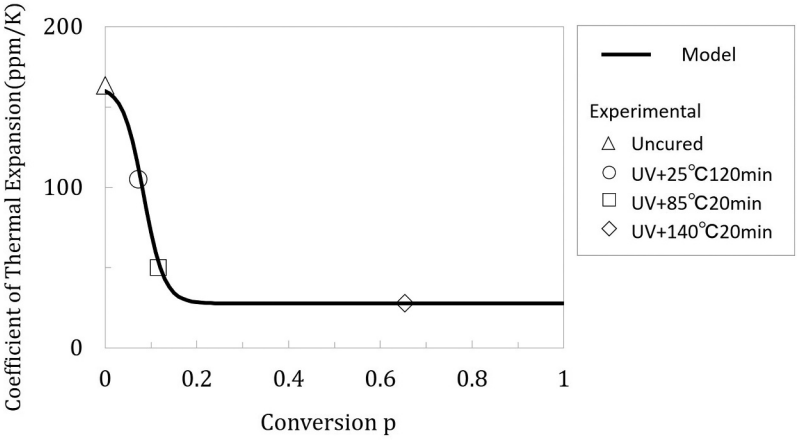

Figure 4. Relationship between the coefficient of thermal expansion and the conversion.

$$S = S_1 \frac{1}{1 + \exp(-B_s(p - p_0))} \tag{10}$$

$$\alpha = (\alpha_0 - \alpha_1) \frac{1}{1 + \exp(-b_\alpha(p - p_0))} + \alpha_1 \tag{11}$$

In Equation 17, S_1 is the shrinkage of the fully cured adhesive and B_S and p_0 are constants determined experimentally. In Equation 17, α_o is the coefficient of linear expansion of the uncured adhesive, α_1 is the coefficient of linear expansion of the fully cured adhesive, and B_α and p_0 are constants to be determined experimentally.

Furthermore, because the adhesive was viscoelastic, its mechanical properties changed over time. Therefore, the long-term relaxation modulus of the adhesive was formulated using the generalized Maxwell

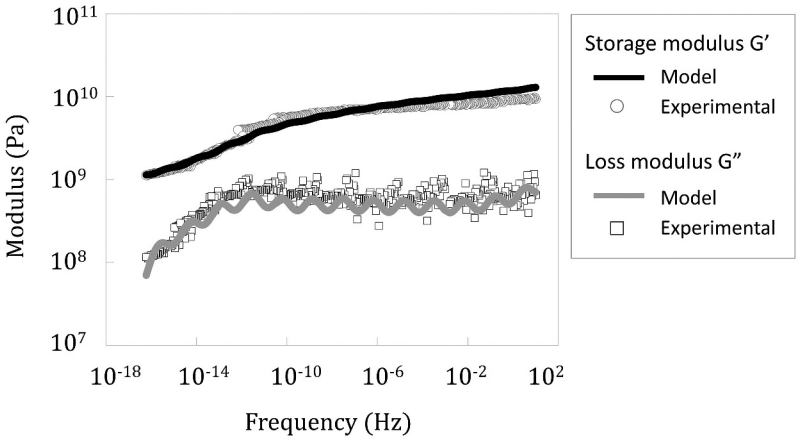

Figure 5. Master curves for storage modulus and loss modulus.

model with the Prony series shown in Equation 17. The frequency characteristics of the viscoelasticity of epoxy resins overlap into a single master curve owing to the horizontal shift of the measurement results obtained at each measurement temperature using the time – temperature superposition law. The relaxation function $\tau_i(T)$ can be obtained using Equation 17, and the amount of horizontal shift (shift factor $a_{\mathrm{H}}(T)$) can be obtained using Equation 17.[27]

$$G(t,T) = G_\infty + \sum_{i=1}^{N} G_i \exp\left(\frac{-t}{\tau_i(T)}\right) \tag{12}$$

$$\tau_i(T) = \frac{1}{\beta_i a_{\mathrm{H}}(\mathrm{T})} \tag{13}$$

$$\log a_{\mathrm{H}}(T) = -\frac{A(T - T_{\mathrm{ref}})}{B + (T - T_{\mathrm{ref}})} \tag{14}$$

Here, t is the time, T_{ref} is the reference temperature, and A and B are constants to be determined experimentally. Frequency dispersion mode DMA measurements (MCR702e, Anton Paar, Austria) of fully cured adhesive samples (30 mm × 10 mm × 0.5 mm) were performed at temperatures of 25–200°C, and the results were used to generate master curves. The master curves for the storage and loss moduli are shown in Figure 5. The relaxation modulus of the adhesive during curing was determined using the ratio of the elastic modulus corresponding to the conversion, as shown in Figure 2.

2.2. Adhesive structure

The adhesive structure discussed in this study is shown in Figure 6 (a). The component (glass S-BSL-7) was bonded to a substrate (oxygen-free copper) using an adhesive. The adhesive part includes not only the adhesive layer at the bottom of the glass component but also fillets formed on the edges of the glass component. Because this adhesive has high viscosity (≃100 Pa·s), the fillet forms the shape as shown in Figure 6(a) when the glass component is placed gently on the adhesive that was applied in a certain amount using a dispenser. The dimensions of the fillet shape shown in Figure 6(a) are measured using the sample after the curing process. We neglected the change of fillet shape and dimensions due to curing because the shrinkage was small. One UV light source was positioned diagonally above the glass component and UV light is irradiated for 500 s. The intensity of the UV light irradiated on the adhesive was not uniform. The UV irradiance of each area is shown in Figure 6(a). The temperatures of the samples measured during curing are shown in Figure 6(b). The adhesive was applied over the thermocouple initially bonded on the copper substrate, and the glass component was placed on the adhesive. The temperature of the adhesive part near the copper substrate was measured by the thermocouple. In addition, the temperature at the surface of the adhesive was monitored with an infrared thermography camera (R300SR-S, Nippon Avionics, Japan). These temperatures and their time variations were similar and their differences were small and negligible. Therefore, in this case, we neglected the effect of temperature on strain and stress.

After UV irradiation, the sample was maintained at 23°C for approximately 90 minutes, which is the upper limit time for measurement using the experimental setup described later. During this time, the curing of the adhesive part progressed owing to a dark reaction. Because the progress of the dark reaction saturates approximately 5 hours after UV irradiation, 90 minutes after UV irradiation corresponds to the middle of the dark reaction. Although the actual manufacturing process involves a post-curing process through heating, this study only concerned the initial curing reaction with UV irradiation (p_{uv}) and the dark reaction after UV irradiation (p_{h1}). The analysis of the deformation associated with post-curing by heating (p_{h2}) is currently underway and is not discussed in this paper.

2.3. Finite element analysis

The implicit solver of the LS-DYNA (version R9.1.0)[1] finite element simulator was used for analysis. The FE model is shown in Figure 7. All parts, including the glass component, the adhesive, and the copper

[1]Any and all ANSYS, Inc. brand, product, service and feature names, logos and slogans such as Ansys, CFX, Fluent are registered trademarks or trademarks of ANSYS, Inc. or its subsidiaries in the United States or other countries.

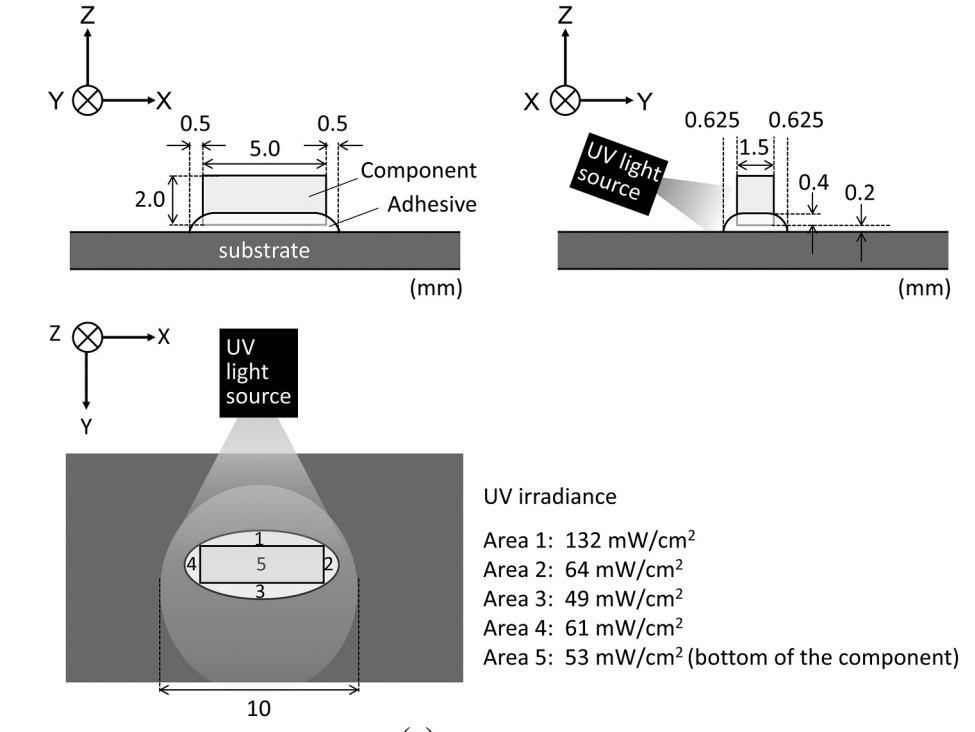

(a)

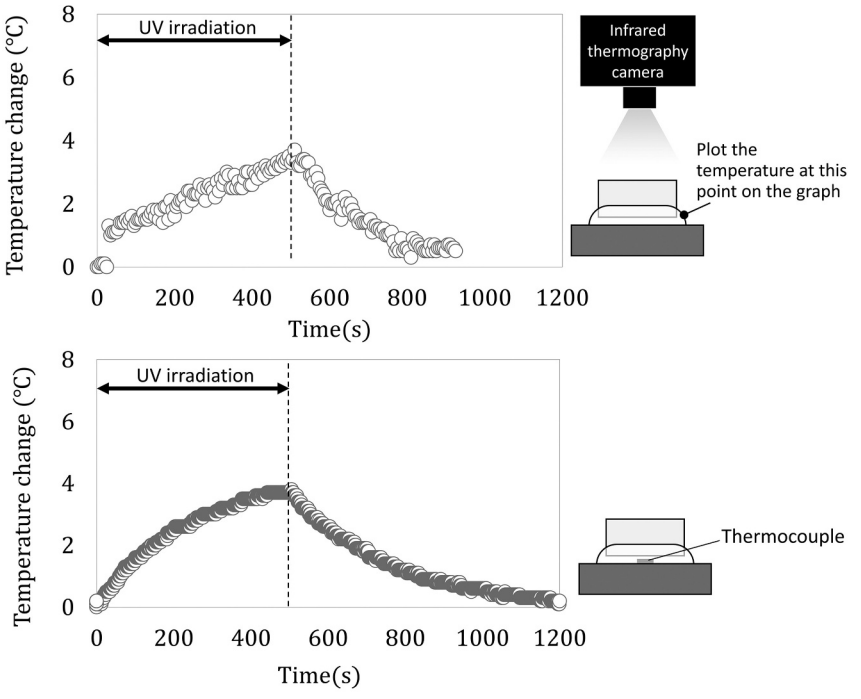

(b)

Figure 6. Adhesive structure for experiments and simulations. (a) Schematic of the adhesive structure, (b) Change in temperature of copper plate surface (Area 5) during UV irradiation.

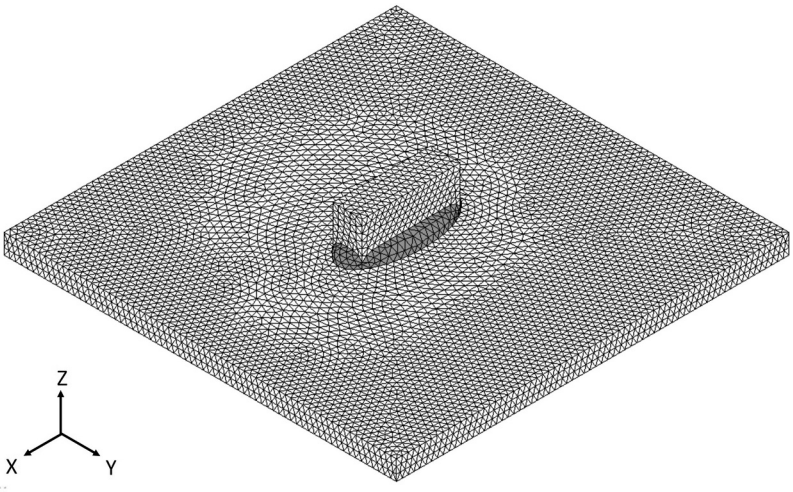

Figure 7. FE model of adhesive structure.

substrate, were divided into similar tetrahedral solid elements with a size of 0.3 mm. Fully integrated S/R solid elements for elements with poor aspect ratio were used for the adhesive, and constant-stress solid elements were used for the glass component and the copper substrate. For the boundary conditions, the adhesive/copper substrate and adhesive/glass component interfaces were assumed to be nodal point sharing, and the Z-direction of the bottom surface of the copper substrate was fixed.

The glass component and copper substrate were treated as elastic bodies that underwent thermal deformation, and the adhesive part was modeled using *MAT_ADHESIVE_CURING_VISCOELASTIC (*MAT_277), a material model in LS-DYNA that can represent the curing of adhesives.[28,29] MAT_277 is a model for heat-cured adhesives but not for UV curing (p_{uv}). Therefore, for the UV curing stage, we calculated the conversion caused through UV irradiance by replacing it with the curing parameters and temperature of the adhesive. Because UV irradiation was not performed in the dark reaction stage (p_{h1}), calculations were performed according to the original usage of MAT_277. The adhesive part was divided into bodies corresponding to areas 1–5 in Figure 6, and the parameters corresponding to each UV irradiance were entered and analyzed.

In MAT_277, the Kamal model was used to calculate the conversion, as in Equation 17 - Equation 17; however, because the n^{th} order model was used in this study, k_2, m, and c_2 were set to zero and converted to Equation 17. This enables the expression of Equation 1, Equation 3, and Equation 5 as

Table 1. List of MAT_277 parameters.

Variable		Value		Significance
		p_{uv}	p_{h1}	
k1	Area 1	7.36×10^{8}	1.00×10^{7}	Parameters of Kamal model
	Area 2	3.51×10^{8}	8.81×10^{6}	
	Area 3	2.69×10^{8}	8.39×10^{6}	(Equation 15 - Equation 17)
	Area 4	3.35×10^{8}	8.73×10^{6}	
	Area 5	2.91×10^{8}	8.51×10^{6}	
k2		0	0	
c1		6.19×10^{7}	6.19×10^{7}	
c2		0	0	
m		0	0	
n		1.00	1.00	
WLFTREF		298.15	298.15	WLF shift function
WLFA		50.0	50.0	
WLAB		400	400	(Equaion 12 - Equation 14)
INCR		1	1	Form of stress calculation 0: Overall form 1: Incremental form

$$\frac{dp}{dt} = (K_1 + K_2 p^m)(1-p)^n \tag{15}$$

$$K_1 = k_1 \exp\left(\frac{-c_1}{RT}\right) \tag{16}$$

$$K_2 = k_2 \exp\left(\frac{-c_2}{RT}\right) \tag{17}$$

$$\frac{dp}{dt} = K_1 (1-p)^n \tag{18}$$

The parameters used in these calculations are listed in Table 1. The modulus of elasticity, curing shrinkage, and linear expansion coefficient at each conversion were input to LS-DYNA as curves based on the model in Section 2.1.

2.4. Experimental in situ measurement of displacement

To prevent influencing the curing process, the measurement must be non-contact, and in such cases, evaluation through image capture is often employed.[30,31] Coherence-scanning interferometer (VertScan R5000, Ryoka Systems, Japan) was used in this experiment. An overview of the experiment is shown in Figure 8. The white light emitted from the light source inside the coherence-scanning interferometer was split into a light flux to the reference mirror and a light flux to the measurement sample by a beam splitter in the objective lens. When the objective lens is scanned in the Z-direction using the piezomechanism, interference fringes are generated around the position wherein the optical path difference between the light flux reflected from the reference mirror and that from the measurement sample is zero. Information

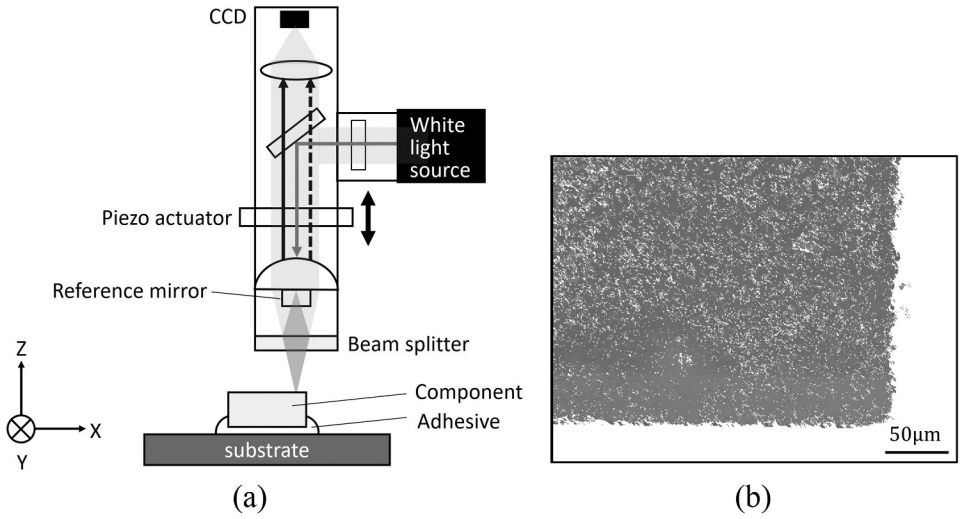

Figure 8. Measuring method for displacements of the glass component. (a) Measurement system for displacements for the glass component, (b) Image acquired using coherence-scanning interferometry.

on the surface shape of the measured sample was obtained by detecting the peak position of the intensity of the interference fringes at each pixel position of the charge-coupled device (CCD) image sensor. Generally, coherence-scanning interferometers are used to measure thin films and surface topography. Moreover, there are also examples of observation of deformation behavior in tensile testing of micro specimens[32] and applications in tribology.[33]

In this study, a coherence-scanning interferometer was used to continuously photograph the top edge of the glass component and acquire images approximately once every 16 s. Measurements were taken from the start of UV irradiation until 90 min after the UV irradiation was stopped. An LED-type UV light source with a central wavelength of 365 nm (LIGHTNINGCURE LC-L1L1V3, Hamamatsu Photonics, Japan) was used for curing. The UV intensity of the samples was measured using a UV illuminance meter (UIT-201, Ushio, Japan). The displacements of the glass components in the X-, Y-, and Z-directions were derived from the captured images. The position in the Z-direction is the average of all pixels at the peak position of the interference fringe intensity. The position in the X- and Y-directions is the average of all pixels at the detected contour position.

3. Results and discussion

The analytical and experimental results of the displacement of the glass component in the XYZ direction are shown in Figure 9. The results indicate similar trends, affirming the efficacy of the proposed

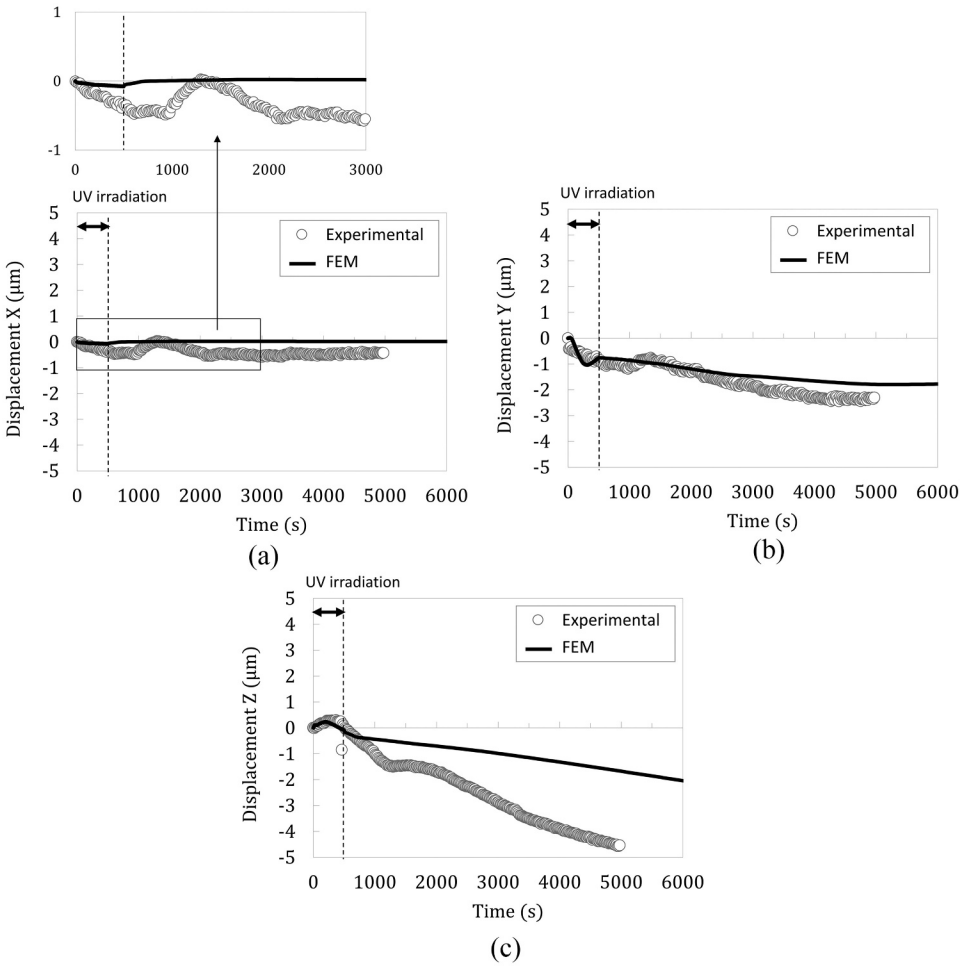

Figure 9. Experimental and simulation results. (a) X-direction displacement, (b) Y-direction displacement, (c) Z-direction displacement.

methodology in predicting curing displacement and facilitating the efficient design of optical components bonded with a specific adhesive, considering the complexities associated with the curing process. However, the displacements were smaller in the analysis than in the experiment. Consequently, this analytical method can be considered qualitative rather than quantitative. One of the possible reasons for the gap between the analysis and the experiment is in the modeling of the conversion. The formulation of the conversion greatly affects the results of the simulation. Especially, the conversion during the dark reaction process should carefully be treated because physical properties change rapidly, but they are still difficult to measure precisely. This topic remains a future challenge for the authors. Another possible reason is the difference in conditions between the analysis and the experiments.

In the analysis, UV irradiation intensity was assumed constant in each area and the distribution in an area was neglected. However, the intensity is actually distributed because of absorbance by the glass component and the adhesive itself. For a more precise analysis, the absorbance should be taken into account. This topic is also a future challenge for the authors.

Notably, most of the glass component displacement occurred during the dark reaction and not during UV irradiation. Moreover, the displacement was gradual over the course of an hour or longer. This is an important aspect to consider in the design of optical products. Both the simulation and experiment showed that the displacement of the glass component during UV irradiation was minimal. This outcome can be attributed to the small values of the elastic modulus and cure shrinkage in the initial stage of curing and approximated that of the uncured state.

Furthermore, it is important to acknowledge that the glass component is displaced not only in the Z-direction, which is the direction of the thickness of the adhesive layer, but also in the Y-direction, which is within the adhesive plane. This phenomenon was probably caused by the non-uniform intensity of UV irradiation. Figure 6(a) illustrates a discrepancy in the UV irradiance between the fillets formed on the two long sides of the glass component. Specifically, one side (Area 1) experienced an irradiance of 132 mW/cm^2, whereas the other side (Area 3) exhibited an irradiance of 49 mW/cm^2: the irradiance of Area 1 is approximately 2.7 times higher than that of Area 3. The curing reaction proceeds faster in Area 1, which is irradiated with intense UV light, and the curing shrinkage and increase in the elastic modulus occur at a faster rate, ultimately causing glass component displacement. The measured displacement in the X-direction after approximately 4,500 s of UV irradiation was 0.4 μm, whereas the measured displacement in the Y-direction was approximately six times larger at 2.4 μm. This discrepancy highlights the necessity of uniform UV irradiation across the entire bonding area to achieve precise positional accuracy.

4. Conclusions

The displacement analysis of an optical component bonded with a cationic polymerized UV-curable epoxy adhesive has been conducted. A curing reaction model was utilized to formulate the conversion, viscoelasticity, expansion, and shrinkage of the adhesive with respect to conversion. These equations, describing the adhesive properties, were then implemented in FEA to predict the movement of the optical component. Concurrently, experiments were performed under identical conditions as the simulation, with continuous

imaging of the optical component using a coherence-scanning interferometer to quantify its displacement.

The FEA and experimental outcomes demonstrate consistent trends, suggesting the applicability of the methodology that combines property modeling and simulation to the manufacturing of optical products. This approach holds potential for reducing product development time while enhancing performance and reliability.

In both the FEA and experiment, it was observed that the displacement of the optical component persisted for several hours, primarily during the dark reaction stage rather than UV irradiation. Furthermore, owing to non-uniform UV intensity within the irradiation area, curing shrinkage was found to occur not only in the direction of adhesive thickness but also in the in-plane direction.

Acknowledgments

The authors express their sincere appreciation to Dr. Koyo Ido (Fujikura Ltd.) for creating the program to analyze the images obtained using a coherence-scanning interferometer. Rheological measurements were performed using a rheometer provided by Anton Paar Japan; we express our deep appreciation for this support.

Disclosure statement

No potential conflict of interest was reported by the author(s).

References

[1] Moon, J. H.; Shul, Y. G.; Han, H. S.; Hong, S. Y.; Choi, Y. S.; Kim, H. T. A Study on UV-Curable Adhesives for Optical Pick-Up: 1.Photo-Initiator Effects. *Int. J. Adhes. Adhes.* 2005, *25*(4), 301–312. DOI: 10.1016/j.ijadhadh.2004.09.003.

[2] Forrer, M.; Strub, H.; Honig, T.; Koller, N.; Kunz, A.; Moser, H.; Brecher, C.; Hoeren, M.; Zontar, D. *High Precision Automated Tab Assembly with Micro Optics for Optimized High-Power Diode Laser Collimation*; SPIE Photonics West: San Francisco California USA, 2020.

[3] Cloppenborg, T. *Precision Alignment for Next Generation Semiconductor Packaging*; SPIE Photonics West: San Francisco California USA, 2023.

[4] Shikama, K.; Aratake, A.; Koike, Y. Analysis of Nano-Creep Deformation of Epoxy Adhesive in Optical Fiber Connector for Long-Term Reliability Prediction. *Optical Fiber Technology*. 2019, *52*, 101975. DOI: 10.1016/j.yofte.2019.101975.

[5] Martin, G. C.; Tungare, A. V.; Fuller, B. W.; Gotro, J. T. Modeling the Structure-Property-Processing Relationships of Epoxy Resins During Cure.47th Annual Technical Conference of Society of Plastics Engineers 1989, New York USA.

[6] Ryan, M. E. Rheological and Heat-Transfer Considerations for the Processing of Reactive Systems. *Polym. Eng. Sci*. 1984, *24*(9), 698–706. DOI: 10.1002/pen.760240912.

[7] Chiou, P. L.; Letton, A. Modelling the Chemorheology of an Epoxy Resin System Exhibiting Complex Curing Behavior. *Polymer*. 1992, *33*(18), 3925–3931. DOI: 10.1016/0032-3861(92)90384-9.
[8] Kamal, M. R. Thermoset Characterization for Moldability Analysis. *Polym. Eng. Sci*. 1974, *14*(3), 231–239. DOI: 10.1002/pen.760140312.
[9] Rogers, A. D.; Sullivan, P. L. An Alternative Model for Predicting the Cure Kinetics of a High Temperature Cure Epoxy Adhesive. *Polym. Eng. Sci*. 2003, *43*(1), 14–25. DOI: 10.1002/pen.10001.
[10] Chern, C. S.; Poehlein, G. W. A Kinetic Model for Curing Reactions of Epoxides with Amines. *Polym. Eng. Sci*. 1987, *27*(11), 788–795. DOI: 10.1002/pen.760271104.
[11] Halley, P. J.; Mackay, M. E. Chemorheology of Thermosets -An Overview. *Polym. Eng. Sci*. 1996, *36*(5), 593–609. DOI: 10.1002/pen.10447.
[12] Wu, J.; Zhao, Z.; Hamel, C. M.; Mu, X.; Kuang, X.; Guo, Z.; Qi, H. J. Evolution of Material Properties During Free Radical Photopolymerization. *J. Mech. Phys. Solids*. 2018, *112*, 25–49. DOI: 10.1016/j.jmps.2017.11.018.
[13] Buback, M.; Huckestein, B.; Russell, G. T. Modeling of Termination in Intermediate and High Conversion Free Radical Polymerizations. Macromol. *Macromol. Chem. Phys*. 1994, *195*(2), 539–554. DOI: 10.1002/macp.1994.021950212.
[14] Golaz, B.; Michaud, V.; Leterrier, Y.; Manson, J.-A. E. UV Intensity, Temperature and Dark-Curing Effects in Cationic Photo-Polymerization of a Cycloaliphatic Epoxy Resin. *Polymer*. 2012, *53*(10), 2038–2048. DOI: 10.1016/j.polymer.2012.03.025.
[15] Corcione, C. E.; Greco, A.; Maffezzoli, A. Time–Temperature and Time-Irradiation Intensity Superposition for Photopolymerization of an Epoxy Based Resin. *Polymer*. 2005, *46*(19), 8018–8027. DOI: 10.1016/j.polymer.2005.06.111.
[16] Decker, C.; Moussa, K. Kinetic Study of the Cationic Photopolymerization of Epoxy Monomers. *J. Polym. Sci.: Part A: Polymer Chemistry*. 1990, *28*(12), 3429–3443. DOI: 10.1002/pola.1990.080281220.
[17] Yu, H.; Adams, R. D.; da Silva, L. F. M. Development of a Dilatometer and Measurement of the Shrinkage Behaviour of Adhesives During Cure. *Int. J. Adhes. Adhes*. 2013, *47*, 26–34. DOI: 10.1016/j.ijadhadh.2013.09.005.
[18] Li, C.; Potter, K.; Wisnom, M. R.; Stringer, G. In-Situ Measurement of Chemical Shrinkage of MY750 Epoxy Resin by a Novel Gravimetric Method. *Compos. Sci. Technol*. 2004, *64*(1), 55–64. DOI: 10.1016/S0266-3538(03)00199-4.
[19] Srirstara, A. K.; White, J. R. Curing Stresses in an Epoxy Polymer. *J. Appl. Polym. Sci*. 1984, *29*(6), 2155–2161. DOI: 10.1002/app.1984.070290621.
[20] Wirries, J.; Vallée, T.; Rütters, M. Cure-Induced Stress Build-Up in Adhesives: Model Building and Parameter Studies. *J. Adhes*. 2022, *99*(9), 1456–1487. DOI: 10.1080/00218464.2022.2121649.
[21] Müller-Pabel, M.; Agudo, J. A. R.; Gude, M. Measuring and Understanding Cure-Dependent Viscoelastic Properties of Epoxy Resin: A Review. *Polym. Test*. 2022, *114*, 107701. DOI: 10.1016/j.polymertesting.2022.107701.
[22] Sato, Y.; Kariya, Y. Cure Shrinkage Behavior Analysis in Ultraviolet Curable Adhesive Using Finite Element Method. 6th International Workshop on Low Temperature Bonding for 3D Integration (LTB-3D), 2019, Kanazawa Japan.
[23] Takahashi, A.; Sekiguchi, Y.; Sato, C. Volume Change and Viscoelastic Properties of UV-Curable Adhesives for Precise Positioning During Curing Process and Their Formulation. *J. Adhes*. 2022, *98*(13), 2029–2044. DOI: 10.1080/00218464.2021.1950538.
[24] Murata, N.; Nishi, S.; Hosono, S. UV-Curable Transparent Adhesives for Fabricating Precision Optical Components. *J. Adhes*. 1996, *59*(1–4), 39–50. DOI: 10.1080/00218469608011075.

[25] Maruno, T.; Murata, N. Properties of a UV-Curable, Durable Precision Adhesive. *J. Adhes. Sci. Technol.* 1995, *9*(10), 1343–1355. DOI: 10.1163/156856195X00031.
[26] Stapp, B.; Schön, L.; Bayer, H.; Hoffmann, M. Photo- and Thermoinitiated Curing of Epoxy Resins by Sulfonium Salts. *Angew. Makromol. Chemie*. 1993, *209*(1), 197–212. DOI: 10.1002/apmc.1993.052090118.
[27] Williams, M. L.; Landel, R. F.; Ferry, J. D. The Temperature Dependence of Relaxation Mechanisms in Amorphous Polymers and Other Glass-Forming Liquids. *J. Am. Chem. Soc*. 1955, *77*(14), 3701–3707. DOI: 10.1021/ja01619a008.
[28] Dong, S.; Smith, A.; Sheldon, A. Modeling of Curing Adhesives Between Jointed Steel and Aluminum Plates Using MAT_277 in LS-DYNA. 11th European LS-DYNA Conference, 2017 Salzburg, Austria.
[29] Agha, A.; Abu-Farha, F. Viscoelastic Model to Capture Residual Stresses in Heat Cured Dissimilar Adhesive Bonded Joints. *Int. J. Adhes. Adhes*. 2021, *107*, 102844. DOI: 10.1016/j.ijadhadh.2021.102844.
[30] Nishikawa, M.; Goto, S.; Hojo, M.; Matsuda, N. In-Situ Observation of Curing and Adhesion Process of Epoxy Resin on a Carbon Fiber and Measurement of Resin Cure Shrinkage Using Microbond Method. *J. Soc. Materials Sci. Japan*. 2018, *67*(4), 416–423.
[31] Jerabek, M.; Major, Z.; Lang, R. W. Strain Determination of Polymeric Materials Using Digital Image Correlation. *Polym. Test*. 2010, *29*(3), 407–416. DOI: 10.1016/j.polymertesting.2010.01.005.
[32] Ito, T.; Mine, Y.; Otsu, M.; Takashima, K. Strain Measurement of Micrometre-Sized Structures Under Tensile Loading by Using Scanning White-Light Interferometry. *Mater. Trans*. 2016, *57*(8), 1252–1256. DOI: 10.2320/matertrans.MG201616.
[33] Cann, P. M.; Spikes, H. A.; Hutchinson, J. The Development of a Spacer Layer Imaging Method (SLIM) for Mapping Elastohydrodynamic Contacts. *Tribol. Trans*. 1996, *39*(4), 915–921. DOI: 10.1080/10402009608983612.